IOPscience iopscience.iop.org

Home Search Collections Journals About Contact us My IOPscience

Temperature–time response of a polymer bonded explosive in compression (EDC37)

This article has been downloaded from IOPscience. Please scroll down to see the full text article.

2008 J. Phys. D: Appl. Phys. 41 085404

(http://iopscience.iop.org/0022-3727/41/8/085404)

View the table of contents for this issue, or go to the journal homepage for more

Download details:
IP Address: 155.198.98.151
The article was downloaded on 25/08/2010 at 16:39

Please note that terms and conditions apply.

J. Phys. D: Appl. Phys. **41** (2008) 085404 (10pp) doi:10.1088/0022-3727/41/8/085404

Temperature–time response of a polymer bonded explosive in compression (EDC37)

D M Williamson[1,4], C R Siviour[2], W G Proud[1], S J P Palmer[1], R Govier[3], K Ellis[3], P Blackwell[3] and C Leppard[3]

[1] University of Cambridge, Department of Physics, Cavendish Laboratory, J J Thomson Avenue, Cambridge, CB3 0HE, UK
[2] University of Oxford, Department of Engineering Science, Parks Road, Oxford OX1 3PJ, UK
[3] AWE Aldermaston, Reading RG7 4PR, UK

E-mail: dmw28@cam.ac.uk

Received 5 December 2007, in final form 13 February 2008
Published 11 March 2008
Online at stacks.iop.org/JPhysD/41/085404

Abstract

The compressive strength of the energetic composition EDC37 has been measured at a temperature of 293 ± 2 K over a range of strain rates from 10^{-8} to 10^{3} s^{-1}, and at a strain rate of 10^{-3} s^{-1} over a range of temperatures from 208 to 333 K. The results show that failure stress is a monotonic function of applied strain rate or temperature, which is dominated by the relaxation properties of the polymeric binder; this is confirmed by dynamic mechanical thermal analysis performed on both EDC37 and its binder. Similarities between the compressive strain rate/temperature data sets can be understood by temperature–time superposition; data collected at a strain rate of 10^{-3} s^{-1} over a temperature range 208 to 333 K were mapped onto a plot of strain rate dependent strength at 293 K, using an empirically determined sensitivity of −13.1 ± 0.3 K per decade of strain rate. Sample size was noted to have a modest effect on the stress–strain behaviour; small length to diameter ratios gave results consistent with an increased degree of confinement. Samples taken to large strains exhibited strain localization in the form of shear bands.

(Some figures in this article are in colour only in the electronic version)

1. Introduction

A principal motivation for this study is the need for experimental data, required to develop and verify computational models to predict the response of the energetic composition EDC37 over its planned life cycle. To date there are limited published experimental data available. The current study addresses this problem by combining compressive data from many experimental techniques, thereby providing a continuous data set covering eleven decades of strain rate (10^{-8}–10^{3} s^{-1}) at a single temperature of 293 K, and additionally over a range of temperatures (208–333 K) at a single strain rate of 10^{-3} s^{-1}.

Data are available on the mechanical properties of tailored Polymer Bonded eXplosive (PBX) compositions designed to discriminate the effects of changing a single characteristic such as binder material, amount of binder, crystal size distribution, etc (Field *et al* 1984, 1985, Pope 1985, Palmer *et al* 1993, Rae *et al* 2002a, Balzer *et al* 2004, Siviour *et al* 2004a). The results show that in general PBXs having a greater binder content undergo greater strains to failure, whilst those with smaller crystal sizes are stronger. The effect of binder type is more difficult to quantify. In a series of experiments carried out at the Cavendish Laboratory, using a combination of white light micrographs and moiré interferometry, it was found that during Brazilian testing of PBXs strain localized in the fine grained binder regions. Upon further loading, tensile failure began simultaneously around the periphery of large filler particles. Such sites then linked up resulting in global failure (Goldrein *et al* 1996, 2002, Rae *et al* 2000, Rae *et al* 2002b, 2002c). These observations indicate that the adhesion between the binder and the filler is likely to be a key parameter in governing the global strengths of such materials.

Despite the wealth of data available on PBXs, it is difficult to collate the compressive strain rate response of a single

[4] Author to whom any correspondence should be addressed.

 © 2008 IOP Publishing Ltd Printed in the UK

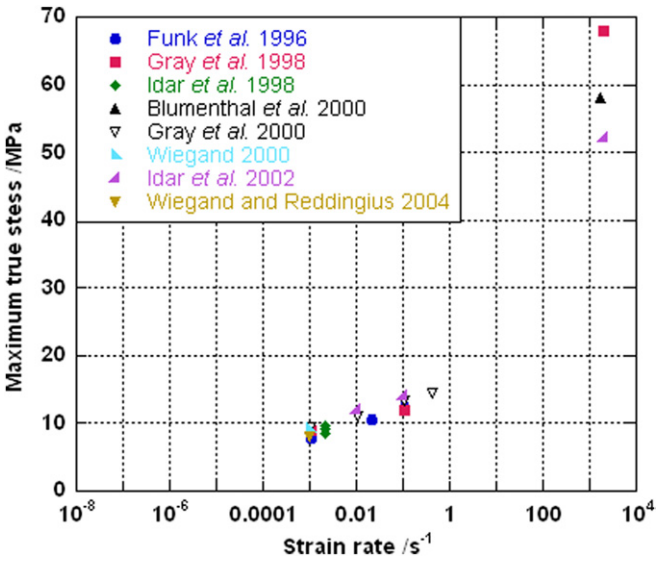

Figure 1. PBX9501 failure stress as a function of strain rate at room temperatures.

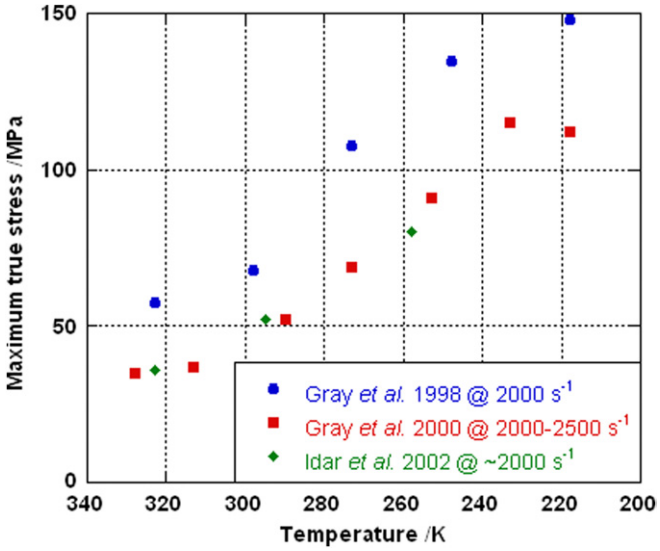

Figure 2. PBX 9501 failure stress as a function of temperature at high strain rates.

composition over a large range; the existing literature tends to be limited to either dynamic rates of the order of $10^3\ s^{-1}$ achieved by drop-weight machines and split Hopkinson pressure bar (SHPB), or else to quasi-static rates of the order of $10^{-3}\ s^{-1}$ achieved with Instron-type material testing machines. Within the published literature, the composition conceptually most akin to EDC37 that has received the most attention, in terms of its compressive strength, is the American composition PBX 9501 (Funk *et al* 1996, Gray *et al* 1998, 2000, Idar *et al* 1998, 2002, Blumenthal *et al* 2000, Wiegand and Reddingius 2004). The main difference between PBX 9501 and EDC37 lies in the binder; EDC37 has a gel-based binder whereas PBX 9501 has a plasticized polyurethane based rubber called Estane 5703. The results for PBX 9501 show increasing strength with increasing strain rate or decreasing temperature. Strains to failure remain almost constant throughout, at a level of approximately 1–3%. Figures 1 and 2 show the totality of the published compressive failure stress data on PBX9501 currently known to the authors.

The results shown in figure 1 look superficially the same as the bilinear response observed of some polymers by Walley and Field (1994).

Experiments on EDC37 by Siviour *et al* (2004b) room temperature and SHPB rates of strain have shown similar stress–strain and strain rate dependent behaviour to PBX 9501, albeit with EDC37 being notably weaker within the regime studied. Ellis *et al* (2005) performed experiments on EDC37 in compression, flexure and tension in an investigation into damage evaluation. Each mode of testing was carried out at a fixed strain rate and temperature.

Dynamic mechanical thermal analysis (DMTA) is a technique that can be used to gain an impression of the relaxation processes in polymers. It has previously been used to investigate PBX and binder properties, most notably by Hoffman (2001, 2003) and references therein.

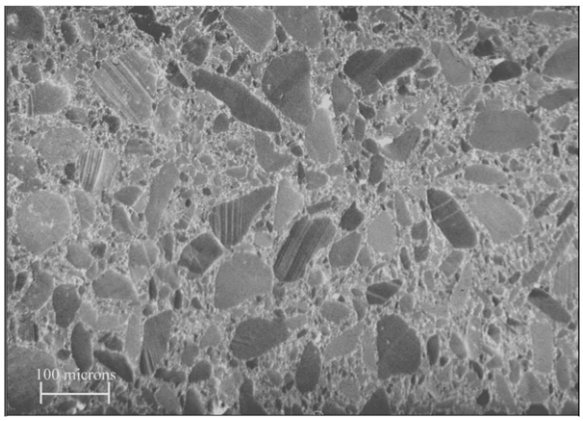

Figure 3. Micrograph of polished EDC37 microstructure.

2. Experimental

2.1. EDC37 Composition

EDC37 is a PBX formed from crystalline cyclotetramethylene tetranitramine (HMX) and a gel-based binder system chosen for its explosive performance and structural properties. The HMX in EDC37 follows a distribution of particle sizes. The majority of particles are 100 μm in diameter, with the remainder being 45 μm in diameter or less. There is also an amount of HMX in the form of small ($<1\ \mu$m) particles (fines). HMX is responsible for 91% of the composition by mass. Figure 3 is an optical micrograph of the structure following sectioning and polishing. The two sizes of particles are clearly visible as are some of the fines. However, the fines are seen better using an atomic force microscope (AFM); see Proud *et al* (2002). The fines are likely to affect both the strength of the binder and possibly the explosive properties of the PBX. Within single crystals of HMX, parallel striations can be seen. These are not artefacts of the polishing, but rather evidence of twins (Palmer and Field 1982) formed either during crystallization, or else by being mechanically

Table 1. Summary of locations, equipment, strain rates and temperatures used in this study.

Location	Equipment	Strain rates (s^{-1})	Temperature (K)
AWE Aldermaston	Creep	10^{-10}–10^{-4}	293 ± 1
AWE Aldermaston	Instron load-hold	5×10^{-8}–5×10^{-7}	293 ± 1
AWE Aldermaston	Slow rate Instron	$5 \times 10^{-6}\,s^{-1}$–5×10^{-3}	293 ± 1
Picatinny Arsenal	MTS	5×10^{-6}–1	$293, 308, 323 \pm 1$
Cavendish	Instron	10^{-4}–1	208 to 333 ± 2
Cambridge Dept. Eng.	Schenk	2–230	293 ± 2
Cavendish	Drop weight	150	293 ± 2
Cavendish	SHPB	200–5×10^{3}	293 ± 2

induced during charge fabrication. The 9% of mass due to the binder is further composed of 13% nitrocellulose and 87% K10 nitro-plasticizer. During production, the binder is introduced to the HMX in the presence of a solvent and then mixed until the solvent evaporates. The resulting binder-coated HMX is then isostatically hot-pressed until the desired density of $1841 \pm 2\,kg\,m^{-3}$ is achieved, which is, within experimental error, the theoretical maximum density of this material. At room temperature the binder material is well above its glass transition temperature of 210 K as measured by differential scanning calorimetry (DSC) (Govier 2000).

2.2. Compressive sample preparation

Samples were prepared from pressed billets of EDC37. Rods were turned on a lathe to the required diameter, and individual samples cut from the rods using a specialised fine-toothed band saw. All samples were inspected after machining, and the parallelism of the ends checked to ensure correct loading of the samples during testing.

2.3. Compressive sample size

In order to obtain data over a wide range of strain rates testing was required at four different locations using seven different machines:

Samples investigated by the Atomic Weapons Establishment (AWE) were standard AWE compression cylinders, length 50.80 mm and diameter 20.27 mm, giving an aspect ratio of 2.5.

Samples at Picatinny Arsenal, New Jersey, were cylinders of length 38.0 mm and diameter 19.0 mm, giving an aspect ratio of 2.0.

Samples at the University of Cambridge were much smaller than those investigated by AWE and Picatinny Arsenal. This was due to the requirements of the SHPB, drop-weight and other high rate experiments to ensure the specimen was in equilibrium during the test and to limit the effects of sample inertia (Gorham 1989, Gray and Blumenthal 2000). The samples were all of 8 mm diameter and varied in length from 2.2 to 5.0 mm, giving aspect ratios of 0.28–0.63.

2.4. Compressive sample temperature

The experiments which were carried out to determine the effect of strain rate were all performed at a temperature of 293 ± 2 K.

The fixed $10^{-3}\,s^{-1}$ strain rate, variable temperature data were obtained with the Cavendish screw-driven Instron machine, using a chamber capable of maintaining a fixed temperature over the range 208 to 333 ± 2 K during the experiment. Additionally, some data were obtained using Picatinny Arsenal's MTS machine at 308 and 323 K and lower strain rates of 5, 50, 500 and $5000 \times 10^{-6}\,s^{-1}$.

2.5. Compressive sample strain rate

The variable strain rate data were obtained at a variety of locations using the following conditions summarized in table 1.

2.5.1. Creep—AWE. The creep experiment operates at very slow strain rates; typically 10^{-10}–$10^{-4}\,s^{-1}$ using bespoke AWE-designed equipment. During a creep experiment an instantaneous load is applied via a pneumatic jack; the sample then remains under this constant load until either the sample fails or the experiment is terminated. The creep apparatus is housed within a thermal chamber that allows the temperature to be accurately controlled to within one kelvin. It should be noted that this arrangement uses a load-control configuration whilst the other experimental techniques described are displacement controlled.

2.5.2. Load-hold method, Instron—AWE. To achieve the slowest strain rates on an Instron test machine located at AWE Aldermaston, a load-hold method was applied. The sample was loaded to a pre-determined strain and this strain was held for a given number of seconds before being incrementally increased. This method produces a saw-tooth stress–strain plot rather than a smooth one. Equivalent strain rates were calculated from a line of best fit to the strain–time plot. Using this methodology, strain rates of 5×10^{-8}–$5 \times 10^{-7}\,s^{-1}$ were achieved. The average of two extensometer outputs were used to control the machine in a strain rate control mode, and record data for analysis.

2.5.3. Slow Rate method, Instron—AWE. An Instron test machine was used to test standard compression cylinders at strain rates ranging from 5×10^{-6} to $5 \times 10^{-3}\,s^{-1}$ using the strain rate control method. The average of two strain gauges was measured, but only one was used to control the machine.

2.5.4. MTS—Picatinny Arsenal, New Jersey. Experiments were carried out on a screw-driven materials test system machine. Samples were tested at strain rates from 5×10^{-6} to $1.0\,s^{-1}$. A linear voltage differential transducer was used to measure axial displacement.

2.5.5. Instron—Cavendish. The Instron at Cambridge is a screw-driven materials testing machine. Strain rates from 1×10^{-4} to $1.0\,s^{-1}$ were used in this investigation. Paraffin wax was used as a lubricant between the sample and the anvil faces; it has previously been shown to be almost ideal, i.e. very low friction when used with samples of polycarbonate (Trautmann *et al* 2005). At the highest strain rates, displacement data were measured using a strain–gauge extensometer mounted across the anvils, and load data were logged on an oscilloscope from the machine's analogue output.

2.5.6. Schenk—Department of Engineering, University of Cambridge. A servo-hydraulic Schenk compression machine was used to obtain stress–strain data between strain rates of 2 and $230\,s^{-1}$, and again paraffin wax was used as a lubricant. Servo-hydraulic testing machines are extremely useful in bridging the strain rates between quasi-static screw-driven Instron-type machines and dynamic drop-weight and SHPB apparatus.

2.5.7. Drop-weight—Cavendish. The drop-weight machine used at Cambridge utilizes a falling mass within the range 5–16 kg from heights of up to 1.6 m, to compress samples between two lubricated anvils. The lower anvil is instrumented with four strain gauges in a configuration which provides temperature compensation. The strain gauges were calibrated to allow force measurements to be made and the standard analysis of twice integrating the acceleration data, taking into account the movement of the upper anvil, was used to obtain displacement data. Triggering is accomplished by making use of a 'make-trigger' circuit formed by the upper anvil and the falling weight. A more detailed description of the apparatus is given by Radford *et al* (2003). High speed photography can be used in conjunction with the drop-weight machine to capture the dynamic deformation of the samples. Some 'classic' explosives research photography, including evidence for ignition by adiabatic shear in explosives, is given by Field *et al* (1982).

2.5.8. Split Hopkinson Pressure Bar—Cavendish. The SHPB used at Cambridge consists of a gas-gun launched striker bar incident upon an input bar, sample, output bar, momentum trap train. The bar materials are chosen to best match the mechanical impedance of the samples in order to maximize the force transmitted by the samples. A more detailed explanation of the results from the SHPB experiments is given by Siviour *et al* (2004b), including confirmation of stress equilibrium in the specimens. It is important to note that the sample does not see the high rate throughout the whole test, i.e. the sample faces undergo rapid acceleration and therefore initial data are collected at a slower rate. This is unlike most of the quasi-static experiments where the specimens see a constant strain rate. However, in line with best practice, it was confirmed that a constant strain rate condition was achieved well before the peak stress was reached in each specimen. For further general discussion of the SHPB and its application to soft materials the reader is referred to Gray III and Blumenthal (2000), and for a broader discussion on high strain rate testing to Field *et al* (2004).

2.6. Dynamic mechanical thermal analysis

Real modulus and $\tan(\delta)$ were measured on a Triton Tritec 2000 dynamic mechanical thermal analyser (DMTA) machine. EDC37 shavings and binder sheet were sandwiched within a steel 'powder-jacket'. The use of powder-jackets permits low sample masses, <100 mg; however, only relative modulus values are obtained. The filled powder jackets were fitted into the DMTA machine and evaluated in a single cantilever bending beam configuration of free span 5 mm. The amplitude and frequency of vibration were 50 μm and 1.0 Hz, respectively. Data were collected over the temperature range from 150 to 420 K.

2.7. Time–temperature superposition

A time–temperature superposition principle was used in order that experimental results could be understood in relative terms: experiments performed at fixed temperature and varied strain rate become conceptually equivalent to fixed strain rate varied temperature experiments (and vice versa)

The physical processes that underlie time–temperature superposition can be identified with molecular motions exhibited by the polymers. Molecular motions are possible only if there is sufficient thermal energy to overcome the potential energy barriers required for movement, and if so will occur with a characteristic temperature dependent frequency and associated time parameter known as a relaxation time. Energy barriers may be described in the simplest terms by the Arrhenius equation.

Given that there is sufficient thermal energy available, then for stimuli applied on time scales greater than the relaxation time the molecules can move in response, resulting in low moduli. However, for stimuli applied on time scales less than the relaxation time the molecules cannot respond, and remain essentially frozen in place, resulting in higher moduli.

The relaxation time is temperature dependent, and it may be understood from simple kinetic theory that relaxation time decreases with increasing temperature. Thus it is clear that a given molecular relaxation can be frozen out either by decreasing the stimuli time scale (increasing strain rate) or reducing the temperature.

The most important relaxation is the one corresponding to large scale chain motion and is known as the glass transition; this separates the glassy from the rubbery regions. Secondary transitions may occur at temperatures below the glass transition and be associated with small scale chain motions, e.g. side chain motion. Providing that it is permitted (no crystallinity or cross-linking), the response to stimuli applied over the longest time scales and highest temperatures is viscous flow.

The most well-known function to describe time–temperature equivalence is that due to Williams, Landel and Ferry (Williams *et al* 1955). The so-called WLF relation describes a shift function $a_T(T, t)$ which relates changes in time to changes in temperature observed in the mechanical properties of viscoelastic solids such as polymers; it is discussed in greater detail within Ferry (1980). The form of the WLF equation most applicable to these data is

$$\Delta \log(\dot{\varepsilon}) = \frac{C_1(T - T_g)}{C_2 + T - T_g}. \quad (1)$$

This equation describes the equivalent isothermal difference in strain rate between two experiments performed at the same strain rate, one at the glass transition temperature T_g and another at an elevated temperature T. When the data are referenced to the glass transition as above, then the constants $C_1 = 17.44$ and $C_2 = 51.6^\circ$ are found to universally apply to a large range of polymers in the range T_g to $(T_g + 100)$ K (Swallowe 1999).

In an investigation by Siviour *et al* (2005) on polycarbonate and polyvinylidene difluoride, the authors investigated the strengths of these materials at strain rates of between 10^{-4} to 1 s^{-1} and 10^3 to 10^5 s^{-1} at room temperature, and -50 to $+150\,^\circ$C at 10^3 s^{-1}, using a combination of an Instron testing machine and Hopkinson bars. Dynamic material analysis data were also taken at several frequencies between temperatures of -100 and 200 °C. It was concluded that the increase in strength observed in each material at high strain rates was due to the shift of low temperature polymer relaxations to room temperatures via a Williams–Landel–Ferry (WLF) type time–temperature superposition relation. Within the range of temperatures and strain rates studied, a value of -17 K per decade of strain rate was found to successfully map the data from variable temperature to variable strain rate for both materials.

Using our collected data, it was possible to graphically measure the apparent change in strain rate, $\Delta \log(\dot{\varepsilon})$, as a function of temperature. The apparent shift in strain rate brought about by a change in temperature is described by the following simple empirical linear equation:

$$\frac{\Delta \log \dot{\varepsilon}}{\Delta T} = \text{constant}. \quad (2)$$

The constant describes the time/temperature sensitivity and was used to map the variable temperature data onto the variable strain rate data.

3. Results and discussion

3.1. Compressive strength as a function of strain rate

Some typical results taken from each experimental set-up are shown in figure 4; creep data are not shown as the comparatively small peak loads measured are not appropriate for this stress range. The oscillations present on the drop-weight data arise from elastic waves travelling through the gauged anvil as various structural components are mechanically excited by the impact.

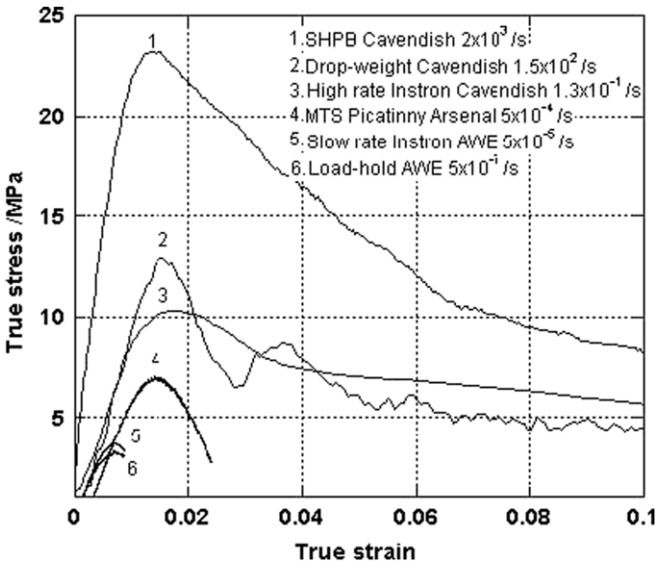

Figure 4. Typical results from the isothermal experimental techniques performed at 293 K.

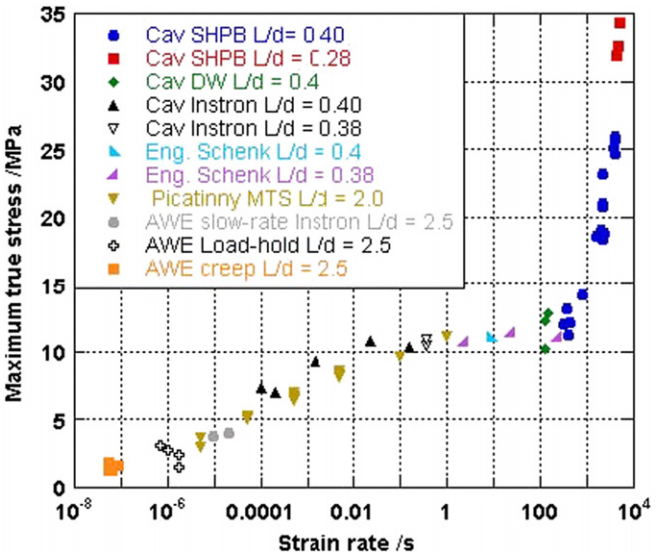

Figure 5. EDC37 failure stress as a function of strain rate tested at 293 K.

It can be seen that the strain at failure increases from approximately 0.5% at the slowest strain rates to 1% at the fastest strain rates.

When all the failure stress data for EDC37 are plotted versus strain rate on a semi-logarithmic plot, figure 5, two linear regions of positive gradient are apparent, and between these two regions a plateau is observed.

It is known that with increasing strain rate the inertia of samples plays an increasing role in the apparent material strength. However, the increase in rate sensitivity seen in figure 5 cannot be explained by inertia; sample sizes were carefully chosen to minimise this effect. Based on expressions derived by Gorham (1989), the inertial forces exhibited by the samples described in this study are negligible; less than 1 part in 5000.

During this series of experiments on EDC37, a small but potentially significant aspect ratio effect was observed.

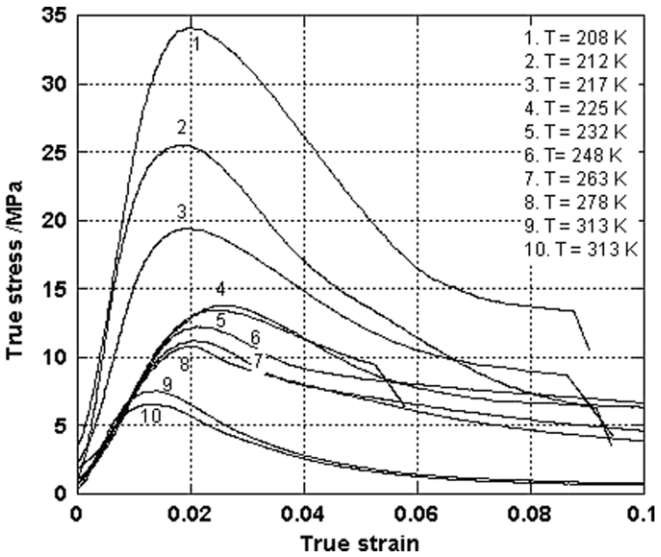

Figure 6. Typical results from the experiments performed at a strain rate of $10^{-3}\,s^{-1}$.

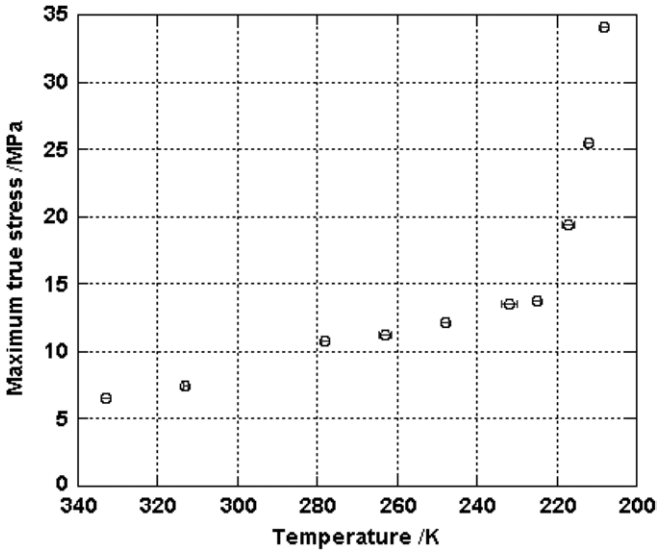

Figure 7. Fixed $10^{-3}\,s^{-1}$ data: failure stress as a function of temperature.

In general, samples tested at low strain rates, less than $1\,s^{-1}$, were of large length/diameter aspect ratio, 2.0–2.5. Those specimens tested at higher rates were necessarily smaller to avoid complications with stress equilibrium and sample inertia, aspect ratios of 0.28–0.63. Where there is overlap in the data between samples of small and large aspect ratios it can be seen that those samples of smaller aspect ratio are apparently stronger. The explanation for this effect is that a reduced aspect ratio results in a greater degree of lateral confinement (Schroeder and Webster 1949). This observation is consistent with the research of Wiegand and Reddingius (2004) which has shown that for PBS 9501 strength increases as a function of hydrostatic confining pressure.

3.2. Compressive strength as a function of temperature

Data from the fixed strain rate, variable temperature experiments on EDC37are shown in figure 6.

It can be seen that the strain at failure increases from approximately 1% at the highest temperatures to 2.5% at intermediate temperatures and reduces to 2% at the coldest temperatures. This greater variation in failure strain, compared with figure 4, is most likely due to thermal contraction/expansion within the samples. This was accounted for to a first approximation by taking the EDC37 contraction/expansion to be equal to the axial average linear coefficient of thermal expansion of HMX; $46.7 \times 10^{-6}\,m\,K^{-1}$ (Menikoff and Sewell 2002). The contraction/expansion due to the 9% by weight of binder is unknown to the authors, and was ignored in calculations of the sample dimensions at temperature.

Failure stress versus temperature data are shown in figure 7 on a linear plot. Note the same general trend as seen in figure 5.

3.3. Evidence of shear band formation during failure

As noted above, EDC37 failed at strains less than 2% in all cases. Failure strains of less than 2% are small in

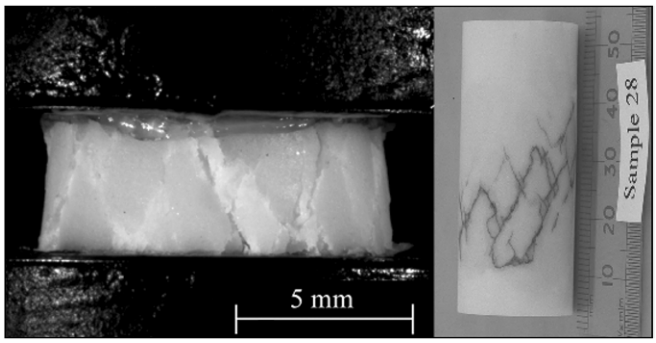

Figure 8. Shear bands observed in quasi-static compression of low and high aspect ratio samples.

polymer terms, but the observed failure was not brittle in nature. Samples taken to large strains showed evidence of strain localization in the form of shear band formation. This observation is important for understanding not only the mechanical behaviour but also the impact sensitivity of the material, since shear bands are recognized to play a role in explosive initiation (Winter and Field 1974, Frey 1981, Swallowe and Field 1981, Field *et al* 1982, Krishna Mohan *et al* 1989, Ho 1992, Dey and Johnson 1998).

Shown in figure 8 are samples exhibiting shear bands at strain rates of $10^{-1}\,s^{-1}$ (left) and $10^{-5}\,s^{-1}$ (right—with added dye penetrant for contrast). Figure 9 shows a sequence of high speed images taken in conjunction with the SHPB in which shear bands are apparent. This indicates that shear banding may appear at all strain rates, but only when taken to large strains. Similarly shear bands were observed at all temperatures.

Shear band formation in polymers is reported by several authors during high strain rate deformation (Winter 1975, Walley 1999), as well as in granular explosives during impact ignition studies as noted above. The extent to which the shear band formation is due to either the polymeric or the granular

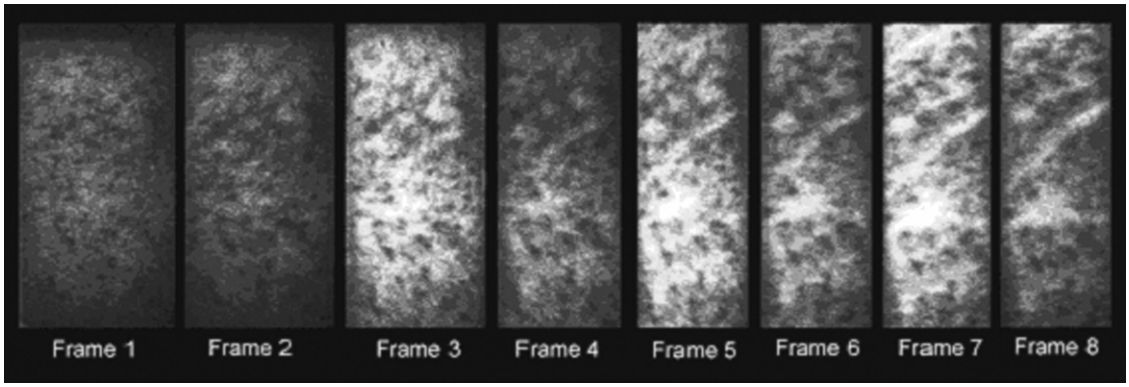

Figure 9. High speed photography of shear bands developing in a SHPB specimen being compressed across its width at $2 \times 10^3\ s^{-1}$, 20 μs interframe time.

components in EDC37 is as yet unknown, although the authors strongly suspect it is due to the granular component.

3.4. Dynamic mechanical thermal analysis

Storage modulus traces, as measured by DMTA performed on both the NC/K10 binder system and EDC37 powder samples are shown in figure 10. The overall trend in each case is the same, and is characteristic of the relaxation processes of an amorphous polymer (Hourston 1999). As both traces follow the same trends it indicates that the presence of HMX plays little role in the relaxation properties of EDC37 within the range studied. Within figure 10 region I is the glassy state, region II is the glass transition region, region III is the rubbery plateau and region IV is the melt region. As the temperature begins to increase and the material warms and expands, the tightly compressed molecules localized bond movements can occur and the material develops some toughness. As heating continues, the chains in amorphous regions begin to coordinate large scale motion the material passes through its T_g (region II). Region III rubbery plateau is where large scale chain movements happen until region IV where chain slippage occurs and the polymer undergoes viscous flow/melt. The viscoelastic nature of the binder system means that the glass transition temperature is frequency (strain rate) dependent; hence a higher value is measured by DMTA (220 K) than by DSC (210 K).

Note that the EDC37 curve is somewhat smoother than that of the binder alone. This may be due to the binder in EDC37 experiencing a range of strain rates by virtue of having a range of inter-particle (binder) lengths on the microstructural level.

3.5. Time–temperature superposition

The similarity between failure stress as a function of strain rate (figure 5) and temperature (figure 7) in EDC37 can be explained if there exists a time–temperature relationship.

It is possible to graphically measure the apparent change in strain rate, $\Delta \log(\dot{\varepsilon})$, as a function of temperature, as illustrated by figure 11. This is done for the rising regions of the failure stress curves only, since measurements taken in the plateau region are ambiguous in the direction of the shift.

Figure 12 shows $\Delta \log(\dot{\varepsilon})$ as a function of temperature, with the classic WLF curve for comparison using a T_g of 210 K. It can be seen that the measured data are much more linear than the WLF equation would predict. As in the case of Siviour *et al* (2005), a linear fit to the data is justifiable. The errors shown were calculated in a least squares fashion.

As described by equation (2), a time/temperature sensitivity of -13.1 ± 0.3 K per decade of strain rate was found to describe the data. This value allows the variable temperature data to be mapped on to the variable strain rate data: see figure 13. It can be seen that the mapping is successful over all the strain rates concerned. Data points 1–4 are highlighted as they use lower aspect ratio samples than the surrounding data, see figure 5. As already argued, one would expect to see a slight increase in strength due to the lower aspect ratio, and points 1–4 are indeed at a higher stress value than surrounding data points.

3.6. Implication of an approximately constant failure strain

Commonly seen in PBX systems are failure strains that are relatively insensitive to strain rate and temperature. This observation leads Wiegand (2003) to speculate about a 'constant global-strain to failure' criterion. Wiegand argues that the damage function is dependent only on strain, and not on temperature/strain rate.

The consequence of an insensitive failure strain is that, to a first approximation, the failure stress becomes proportional to the storage modulus. Hence the similarity between the DMTA results of figure 10, and failure stresses as a function of temperature and strain rate. By extrapolation, the DMTA results lead us to believe that the failure stresses observed in figures 5 and 7 will not continue to infinity with increasing strain rate or decreasing temperature, but rather will level off once the binder response becomes fully glassy.

The interpretation is therefore that the compressive failure stress envelopes of EDC37 as functions of both strain rate and temperature are governed by the relaxation properties of the NC/K10 binder system and they are made equivalent by a factor of 13.1 ± 0.3 K per decade of strain rate.

It is important to note that in the above no mention is made of what dictates the absolute value of failure stress; that is a complicated function of both the properties of the HMX and the binder.

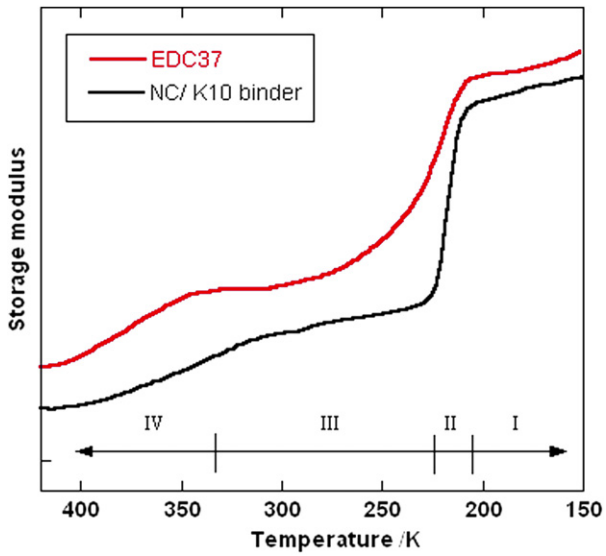

Figure 10. Storage modulus DMTA traces of NC/K10 binder and EDC37 powder samples. Region I is the glassy state, region II is the glass transition region, region III is the rubbery plateau and region IV is viscous flow.

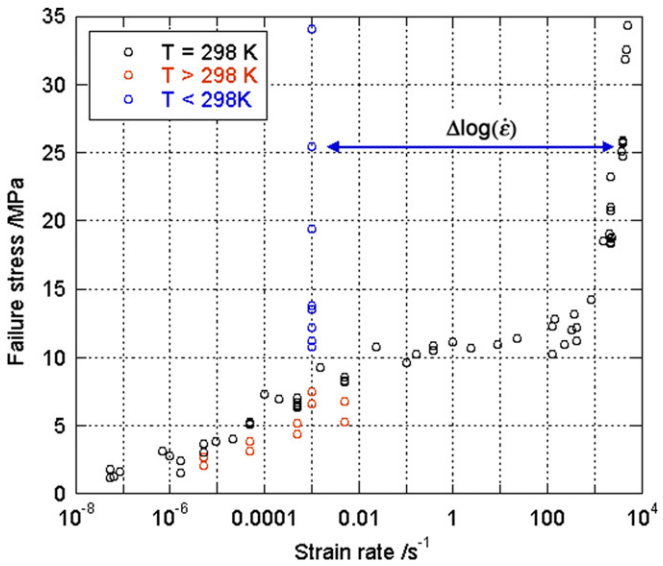

Figure 11. Graphical measure of $\Delta \log(\dot{\varepsilon})$.

3.7. Limitations of time–temperature equivalency

Currently no analytical function exists to describe the form of the failure stress curves. However by using the collected data set it is now possible to predict the ultimate failure stress over a large range of temperatures and strain rates by utilizing the time–temperature equivalency.

There are limitations to the time–temperature equivalency analogy. In general, different relaxations may have different time–temperature sensitivities. Changing sample temperature will bring about internal stresses via differential thermal contraction, and this cannot be simulated by appropriate choice of strain rate. Changing the temperature will also change the sample density, which is another variable known to affect strength (Thompson *et al* 2005).

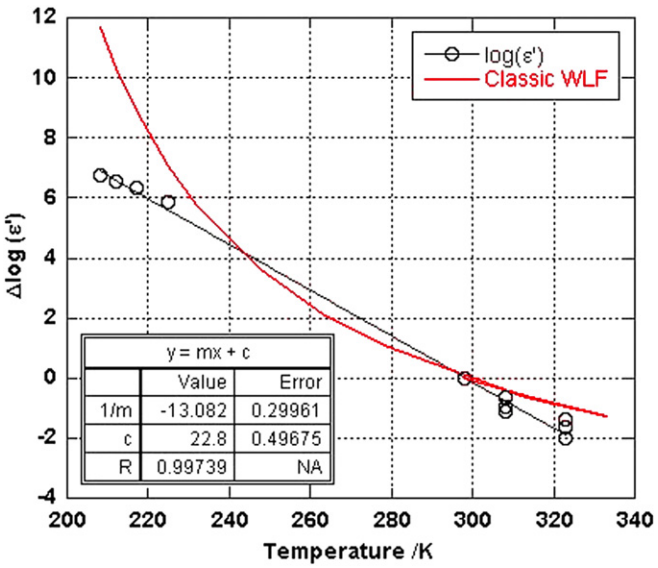

Figure 12. Strain rate shift factor, referenced to T_g, as a function of applied temperature.

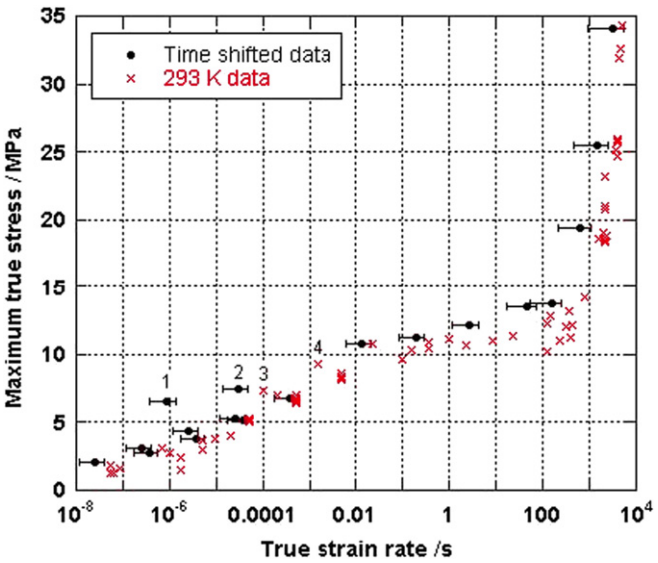

Figure 13. Application of time–temperature superposition principle using a linear transformation of −13.1 kelvin per decade of strain rate. Data points 1–4 are of lower aspect ratio than the surrounding data in this region.

4. Conclusions

Many different techniques performed at various locations have generated a coherent data set that reveals the monotonic nature of the compressive failure stress of EDC37 as a function of applied strain-rate or temperature. The data cover eleven decades of strain rate and 125 K temperature range and should be valuable to future computational modelling efforts. It provides real data on the strain rate regimes as experienced by the material during its whole life cycle against which modelling efforts can be validated.

Within the results there exists a sample size dependence that has its basis in the degree of confinement present; samples of small aspect ratio have apparently higher strengths than

those samples of high aspect ratio.

Photographic evidence shows that shear bands form during failure, and it is well known that shear bands are associated with localized temperature rises and may contribute to the sensitivity of the material to mechanical insult. It is important that any computational models that are developed also capture this behaviour.

It has been shown that the time–temperature superposition principle can be successfully applied to the compressive failure stress of EDC37, and that the shift function within the range of strain rates and temperatures studied is essentially linear. Using a value of -13.1 ± 0.3 K per decade of strain rate the fixed strain rate data were mapped on to the fixed temperature data. The classic WLF function, with the 'standard' constants, is not suitable.

The potential benefit of a time–temperature superposition approach in further research is that if the principle can be applied with confidence, then all the required experiments to map out a materials response can be made on a single test machine with a limited strain rate range on which the temperature of testing is controllable, thus negating the large number of experimental approaches currently needed to map out strain rate response over a practically useful range.

A cautionary note should be added; in general the temperature–time sensitivity of each relaxation will be different and a linear mapping as above can only be expected to work within a finite regime. Furthermore, certain physical effects brought about by the application of temperature, for example the degree of internal stress due to differential thermal expansion, cannot be reproduced by appropriate choice of strain rate.

DMTA has been performed on both EDC37 powder samples and NC/K10 binder. The results show that within the range of temperatures studied, the presence of HMX has little effect on the temperatures at which polymer relaxation processes occur.

The compressive failure stress envelope of EDC37 has been shown to be dominated by the relaxation properties of the binder system, despite the fact that its contribution to the composition is only 9% by mass. The high degree of correlation that exists between the trends of failure stress and those of DMTA is due to a failure strain which is relatively insensitive to the effects of time and temperature.

Acknowledgments

The authors would like to thank EPSRC for studentships for D M Williamson and C R Siviour and grants for the high speed cameras. They would also like to thank AWE Aldermaston for samples, data, discussion and funding. D Wiegand of Picatinny Arsenal is thanked for performing the experiments there. W G Proud is QinetiQ Senior Research Fellow at the Cavendish Laboratory. C R Siviour would like to thank the Worshipful Company of Leathersellers for funding. Professor J E Field is thanked for his valuable advice and comments. R Flaxman and D Johnson of the Cavendish Laboratory's workshop are thanked for technical assistance.

© British Crown Copyright 2008/MOD

References

Balzer J E, Siviour C R, Walley S M, Proud W G and Field J E 2004 Behaviour of ammonium perchlorate-based propellants and a polymer-bonded explosive under impact loading *Proc. R. Soc. Lond.* A **460** 781–806

Blumenthal W R, Gray III G T, Idar D J, Holmes M D, Scott P D, Cady C M and Cannon D D 2000 Influence of temperature and strain rate on the mechanical behaviour of PBX 9502 and Kel-F 800 *Shock Compression of Condensed Matter—1999* ed M D Furnish *et al* (Melville, NY: American Institute of Physics) pp 671–4

Dey T N and Johnson J N 1998 Shear band formation in plastic bonded explosive (PBX) *Shock Compression of Condensed Matte—1997* ed S C Schmidt *et al* (Woodbury, NY: American Institute of Physics) pp 285–8

Ellis K, Leppard C and Radesk H 2005 Mechanical properties and damage evaluation of a UK PBX *J. Mater. Sci.* **40** 6241–8

Ferry J D 1980 *Viscoelastic Properties of Polymers* (New York: Wiley)

Field J E, Swallowe G M and Heavens S N 1982 Ignition mechanisms of explosives during mechanical deformation *Proc. R. Soc. Lond.* A **382** 231–44

Field J E, Swallowe G M, Pope P H and Palmer S J P 1984 High strain rate properties of explosives *Inst. Phys. Conf. Ser.* **70** 381–8

Field J E, Palmer S J P, Pope P H, Sundararajan R and Swallowe G M 1985 Mechanical properties of PBX's and their behaviour during drop weight impact *Proc. 8th Symp. (Int.) on Detonation* ed J M Short (White Oak, MD: Naval Surface Weapons Center) pp 635–44

Field J E, Walley S M, Proud W G, Goldrein H T and Siviour C R 2004 Review of experimental techniques for high rate deformation and shock studies *Int. J. Impact Eng.* **30** 725–75

Frey R B 1981 The initiation of explosive charges by rapid shear *Proc. 7th Symp. (Int.) on Detonation* ed J M Short (White Oak, MD: Naval Surface Weapons Center) pp 36–42

Funk D j, Laabs G W, Peterson P D and Asay B W 1996 Measurement of the stress/strain response of energetic materials as a function of strain rate and temperature: PBX 9501 and Mock 9501 *Shock Compression of Condensed Matter—1995* ed S C Schmidt, W C Tao (Woodbury, NY: American Institute of Physics) pp 145–8

Goldrein H T, Palmer S J P and Huntley J M 1996 Microstructural analysis of composites using high magnification moiré interferometry *Proc. Applied Optics Division Conf.* (London: Institute of Physics) pp 10–15

Goldrein H T, Rae P J, Palmer S J P and Field J E 2002 Construction of a high-resolution moiré interferometer for investigating microstructural displacement fields in materials *Phil. Trans R. Soc. Lond.* A **360** 939–52

Gorham D A 1989 Specimen inertia in high strain rate experiments *J. Phys. D: Appl. Phys.* **22** 1888–93

Govier R 2000 The study of thermally induced phase transitions in a Nitrocellulose and K10 polymer binder system *Degree Thesis* Brunel University and Trowbridge College

Gray G T III and Blumenthal W R 2000 Split-Hopkinson pressure bar testing of soft materials *ASM Handbook. (vol 8: Mechanical Testing and Evaluation)* ed H Khun and D Medlin (Materials Park, OH: ASM International) pp 488–96

Gray G T III, Blumenthal W R, Idar D J and Cady C M 1998 Influence of temperature on the high-strain rate mechanical behaviour of PBX 9501 *Shock Compression of Condensed Matter—1997* ed S C Schmidt *et al* (Woodbury, NY: American Institute of Physics) pp 583–6

Gray G T III, Idar D J, Blumenthal W R, Cady C M and Peterson P D 2000 High- and low-strain rate compression properties of several energetic material composites as a function of strain rate and temperature *Proc. 11th Symp. (Int.)*

on Detonation ed J M Short and J E Kennedy (Arlington, VA: Office of Naval Research) pp 76–84
Ho S Y 1992 Impact ignition mechanisms of rocket propellants *Combust. Flame* **91** 131–42
Hoffman D M 2001 Dynamic mechanical signatures of a polyester–urethane and plastic-bonded explosive based on this polymer *J. Appl. Polym. Sci.* **83** 1009–24
Hoffman D M 2003 Dynamic mechanical signatures of Viton A and polymer bonded explosives based on this polymer *Polym. Eng. Sci.* **43** 139–54
Hourston D J 1999 Glass transition *Mechanical Properties and Testing of Polymers, An A-Z Reference* ed G M Swallowe (Dordrechht: Kluwer) pp 109–12
Idar D J, Peterson P D, Scott P D and Funk D J 1998 Low strain rate compression measurements of PBXN-9, PBX 9501 and Mock 9501 *Shock Compression of Condensed Matter—1997* ed S C Schmidt *et al* (Woodbury, NY: American Institute of Physics) pp 587–90
Idar D J, Thompson D G, Gray III G T, Blumenthal W R, Cady C M, Peterson P D, Roemer E L, Wright W J and Jacquez B L 2002 Influence on polymer molecular weight, temperature, and strain rate on the mechanical properties of PBX 9501 *Shock Compression of Condensed Matter—2001* ed M D Furnish *et al* (Melville, NY: American Institute of Physics) pp 281–4
Krishna Mohan V, Bhasu V C J and Field J E 1989 Role of adiabatic shear bands in initiation of explosives by drop-weight impact *Proc. 9th Symp. (Int.) on Detonation* (Arlington, VA: Office of Naval Research) pp 1276–83
Menikoff R and Sewell T D 2002 Constituent properties of HMX needed for mesoscale simulations *Combust. Theory Modelling* **6** 103–25
Palmer S J P and Field J E 1982 The deformation and fracture of β-HMX *Proc. R. Soc. Lond.* A **383** 399–407
Palmer S J P, Field J E and Huntley J M 1993 Deformation, strengths and strains to failure of polymer bonded explosives *Proc. R. Soc. Lond.* A **440** 399–419
Pope P H 1985 Dynamic compression of metals and explosives *PhD Thesis* University of Cambridge
Proud W G, Palmer S J P, Field J E, Kennedy G and Lewis A L 2002 AFM studies of PBX systems *Thermochim. Acta* **384** 245–51
Radford D D, Walley S M, Church P and Field J E 2003 Dynamic upsetting and failure of metal cylinders: experiments and analysis *J. Phys. IV France* **110** 263–8
Rae P J, Goldrein H T, Palmer S J P, Field J E and Lewis A L 2000 Studies of the failure mechanisms of polymer bonded explosives by high resolution moiré interferometry and environmental scanning electron microscopy *Proc. 11th Symp. (Int.) on Detonation* ed J M Short and J E Kennedy (Arlington, VA: Office of Naval Research) pp 66-75
Rae P J, Palmer S J P, Goldrein H T, Field J E and Lewis A L 2002a Quasi-static studies of β-HMX based polymer bonded explosives *Proc. R. Soc. Lond.* A **458** 743–62
Rae P J, Palmer S J P, Goldrein H T, Field J E and Lewis A L 2002b Quasi-static studies of the deformation and failure of PBX 9501 *Proc. R. Soc. Lond.* A **458** 2227–42
Rae P J, Goldrein H T, Palmer S J P and Proud W G 2002c Moiré interferometry studies of PBX 9501 *Shock Compression of Condensed Matter—2001* ed M D Furnish *et al* (Melville, NY: American Institute of Physics) pp 825–8
Schroeder W and Webster D A 1949 Press-forging thin section: effect of friction, area, and thickness on pressures required *J. Appl. Mech.* **16** 289–94
Siviour C R, Gifford M J, Walley S M, Proud W G and Field J E 2004a Particle size effects on the mechanical properties of a polymer bonded explosive *J. Mater. Sci.* **39** 1255–8
Siviour C R, Williamson D M, Grantham S G, Palmer S J P, Proud W G and Field J E 2004b Split Hopkinson Bar Measurements of PBXs *Shock Compression of Condensed Matter—2003* ed M D Furnish *et al* (Melville, NY: American Institute of Physics) pp 804–7
Siviour C R, Walley S M, Proud W G and Field J E 2005 The high strain rate compressive behaviour of polycarbonate and polyvinylidene difluoride *Polym.* **46** 12546–55
Swallowe G M 1999 Time-temperature equivalence *Mechanical Properties and Testing of Polymers, An A–Z Reference* ed G M Swallowe (Dordrechht: Kluwer) pp 249–51
Swallowe G M and Field J E 1981 The ignition of a thin layer of explosive by impact; the effect of polymer particles *Proc. R. Soc. Lond.* A **379** 389–407
Thompson D G, Olinger B and DeLuca R 2005 The effect of pressing parameters on the mechanical properties of plastic bonded explosives *Propellants, Explosives, Pyrotechn.* **30** 391–6
Trautmann A, Siviour C R, Walley S M and Field J E 2005 Lubrication of polycarbonate at cryogenic temperatures in the split Hopkinson pressure bar *Int. J. Impact Eng.* **31** 523–44
Walley S M 1999 Adiabatic shear instability: observations and experimental techniques *Mechanical Properties and Testing of Polymers* ed G M Swallowe (Dordrechht: Kluwer) pp 10–14
Walley S M and Field J E 1994 Strain rate sensitivity of polymers in compression from low to high rates *DYMAT J.* **1** 211–27
Wiegand D A 2000 Mechanical failure of composite plastic bonded explosives and other energetic materials *Proc. 11th Symp. (Int.) on Detonation* ed J M Short and J E Kennedy (Arlington, VA: Office of Naval Research) pp 744–50
Wiegand D A 2003 Constant strain criteria for mechanical failure of energetic materials *J. Energetic Mater.* **21** 109–24
Wiegand D and Reddingius B 2004 Mechanical properties of plastic bonded composites as a function of hydrostatic pressure *Shock Compression of Condensed Matter* ed M D Furnish *et al* (Melville, NY: American Institute of Physics) pp 812–5
Williams M L, Landel R F and Ferry J D 1955 The temperature dependence of relaxation mechanisms in amorphous polymers and other glass-forming liquids *J. Am. Chem. Soc.* **77** 3701–7
Winter R E 1975 Adiabatic shear of titanium and polymethylmethacrylate *Phil. Mag.* **31** 765–73
Winter R E and Field J E 1974 The role of localized plastic flow in the impact initiation of explosives *Proc. R. Soc. Lond.* A **343** 399–413